Available online at www.sciencedirect.com
ScienceDirect
Coordination Chemistry Reviews 251 (2007) 515–524
COORDINATION CHEMISTRY REVIEWS
www.elsevier.com/locate/ccr

Review

Electronic structure, spectroscopy, and photochemistry of group 8 metallocenes

Yoshikazu Yamaguchi, Wei Ding, Cynthia T. Sanderson, Michelle L. Borden, Matthew J. Morgan, Charles Kutal *

Department of Chemistry, University of Georgia, Athens, GA 30602, United States

Received 19 December 2005; accepted 21 February 2006
Available online 30 March 2006

Contents

Abstract

Spectral and photochemical studies of ferrocene, ruthenocene, and several of their benzoyl-substituted derivatives have provided valuable information about the electronic structures and excited state reactivities of these group 8 metallocenes. The presence of a benzoyl group on one or both cyclopentadienyl rings of the metallocene strongly influences the electronic transitions observed in the UV–vis spectral region. While the parent complexes display low-intensity, solvent-insensitive ligand field absorption bands, the monobenzoyl and 1,1′-dibenzoyl derivatives exhibit bands that are much more intense and sensitive to the solution environment. This behavior results from the mixing of appreciable metal-to-ligand charge transfer (MLCT) character into the low-energy excited states of the benzoyl-substituted complexes. Resonance Raman data lend strong support to this MLCT assignment. Irradiation of a metallocene dissolved in ethyl 2-cyanoacrylate results in the anionic polymerization of the electrophilic monomer. Studies of the kinetics and mechanism of this photoinitiated polymerization process reveal that it occurs by two competing charge transfer-induced pathways, the relative importance of which depends upon the identity of the metal and the presence or absence of the benzoyl substituent.

Keywords: Metallocenes; Ferrocene; Ruthenocene; Photoinitiated polymerization

1. Introduction

Five decades have passed since the discovery of ferrocene [1,2], $Fe(\eta^5\text{-}C_5H_5)_2$ (Fc in Fig. 1), yet interest in this remarkable organometallic compound shows no signs of waning. The initial reports of the existence of a thermally stable compound containing only iron, carbon, and hydrogen caused a spate of studies that established its unique sandwich molecular structure, strong metal-ring π bonding, facile redox behavior, and ease of derivatization [3]. A diverse assortment of ferrocene derivatives have been prepared and recent work has focused on the applications of these compounds in areas such as homogeneous catalysis, polymer chemistry, molecular sensing, and nonlinear optical materials [4].

* Corresponding author. Tel.: +1 706 542 0012; fax: +1 706 542 9454.
E-mail address: ckutal@chem.uga.edu (C. Kutal).

0010-8545/$ – see front matter © 2006 Elsevier B.V. All rights reserved.
doi:10.1016/j.ccr.2006.02.028

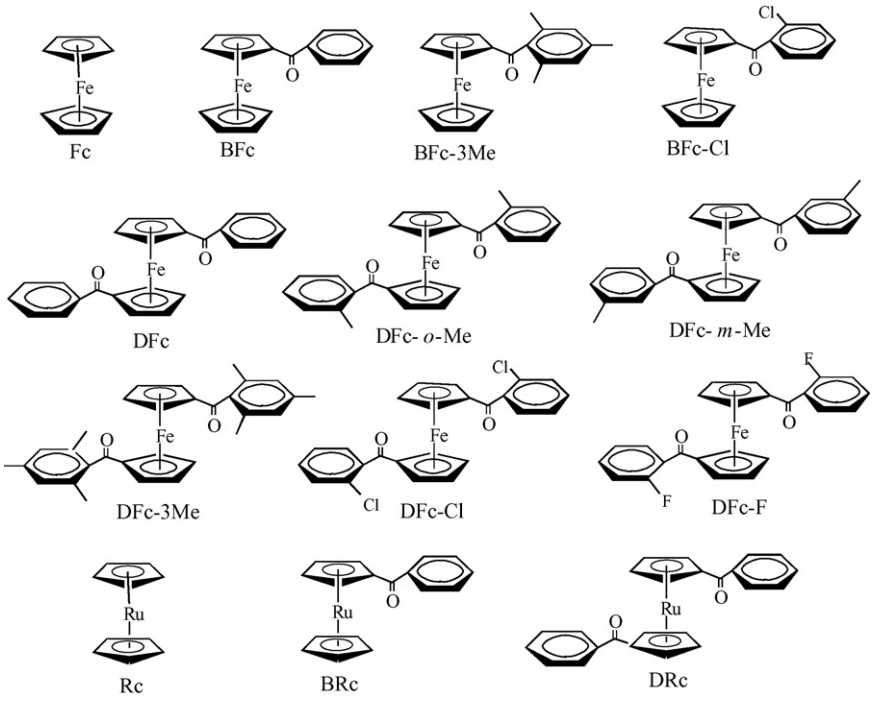

Fig. 1. Structures of group 8 metallocenes.

Several studies from this laboratory have explored the use of Fc and other group 8 metallocenes as photoinitiators for the polymerization of epoxy and acrylate monomers [5–10]. While the detailed mechanism of photoinitiated polymerization depends upon the chemical composition of the system (e.g. monomer, photoinitiator, solvent) and the experimental conditions employed (e.g. excitation wavelength), in general, the overall process can be dissected into two essential steps [11]. Initially, the absorption of a photon by the photoinitiator, PI, results in the photochemical generation of one or more reactive species, IN (Eq. (1)). In a subsequent thermal step, IN reacts with the monomer to initiate polymer formation (Eq. (2)).

$$\mathrm{PI} \xrightarrow{h\nu} \mathrm{IN} \tag{1}$$

$$\mathrm{IN} + \text{monomer} \rightarrow \text{polymer} \tag{2}$$

For the vast majority of reported photoinitiators, IN is a radical or a strong acid [12,13]. In contrast, we have found that Fc and several of its derivatives generate an anionic initiating species when irradiated in solutions containing an alkyl 2-cyanoacrylate monomer. Our results indicate that this photochemical process can occur by two distinct pathways that originate in electronic excited states of different orbital parentage. In succeeding sections of this article we present spectroscopic and photochemical evidence that has allowed us to characterize these excited states and elucidate the mechanisms by which they react to generate anions. For comparison, we also describe results obtained for the analogous ruthenocene compounds.

2. Spectroscopy and photochemistry of unsubstituted group 8 metallocenes

2.1. Ferrocene

This prototypical metallocene adopts a sandwich structure (Fig. 1), with only a small energy barrier separating the staggered (D_{5d} symmetry) and eclipsed (D_{5h} symmetry) rotational orientations of the parallel cyclopentadienyl rings [14]. Important features of the electronic structure and spectroscopy of Fc can be described by reference to the qualitative molecular orbital diagram in Fig. 2 [15,16]. In idealized D_{5d} symmetry, the 10 pπ orbitals of the two rings form the symmetry-adapted combinations a_{1g}, a_{2u}, e_{1g}, e_{1u}, e_{2g}, and e_{2u}. Interaction of these ligand-centered orbitals with the metal 3d, 4s, and 4p valence atomic orbitals of appropriate symmetry generates the molecular orbitals shown in the center of the diagram. The best overlap occurs between the ligand e_{1g} set and the $3d_{xz}$,$3d_{yz}$ orbitals. The resulting $1e_{1g}$ molecular orbitals are mostly ligand in character, strongly bonding, and filled with two pairs of electrons, while the corresponding $2e_{1g}{}^{*}$ antibonding orbitals are predominantly metal in character and unoccupied. Poor δ-type overlap between the $3d_{x2-y2}$,$3d_{xy}$ orbitals and the e_{2g} ring orbitals leads to weak bonding, and, as a consequence, the filled $1e_{2g}$ molecular orbitals retain a large percentage of metal character. The near-zero overlap of the $3d_{z2}$ and ligand a_{1g} orbitals results in a nonbonding, essentially pure metal molecular orbital, $2a_{1g}$, that contains two electrons and is the highest occupied level in the complex.

Because the $1e_{2g}$, $2a_{1g}$, and $2e_{1g}{}^{*}$ molecular orbitals contain substantial metal 3d orbital character, we can treat the low-lying electronic transitions of Fc within the formalism of ligand field theory [15,17]. The $^{1}A_{1g}$ ground state of this $3d^{6}$

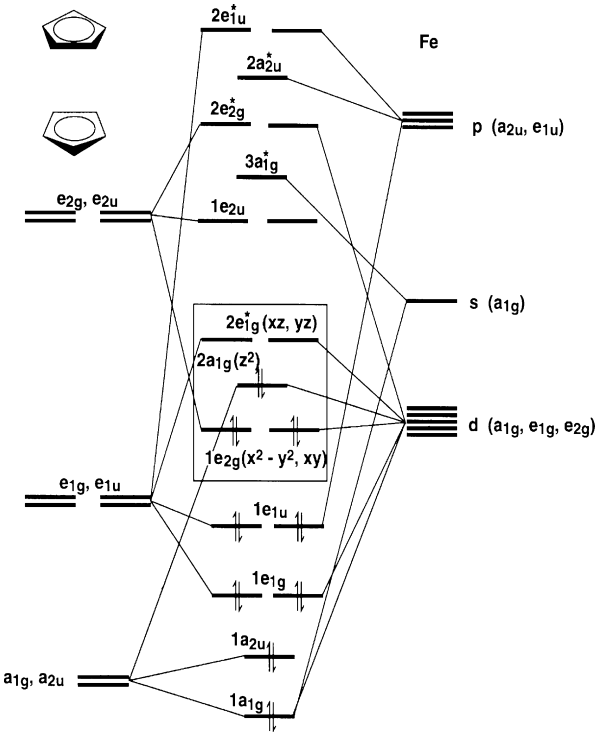

Fig. 2. Qualitative molecular orbital diagram for ferrocene. Box encloses the molecular orbitals that contain appreciable metal d-orbital character. Reproduced from Ref. [26]. Copyright 1997 American Chemical Society.

metallocene arises from the $(1e_{2g})^4(2a_{1g})^2(2e_{1g}^*)^0$ electronic configuration. Photoexcitation of a $2a_{1g}$ electron to the empty $2e_{1g}^*$ orbitals produces an E_{1g} excited state, while E_{2g} and E_{1g} excited states result from photoexcitation of a $1e_{2g}$ electron to the $2e_{1g}^*$ orbitals. Accordingly, three spin-allowed ligand field transitions are expected: $^1A_{1g} \rightarrow a^1E_{1g}$, $^1A_{1g} \rightarrow {}^1E_{2g}$, and $^1A_{1g} \rightarrow b^1E_{1g}$. The first two transitions are unresolved and give rise to the band at 442 nm in the absorption spectrum of Fc in room-temperature tetrahydrofuran (Fig. 3, spectrum a). The third transition is responsible for the band at 325 nm. Both bands are weak owing to the Laporte-forbidden d–d character of ligand

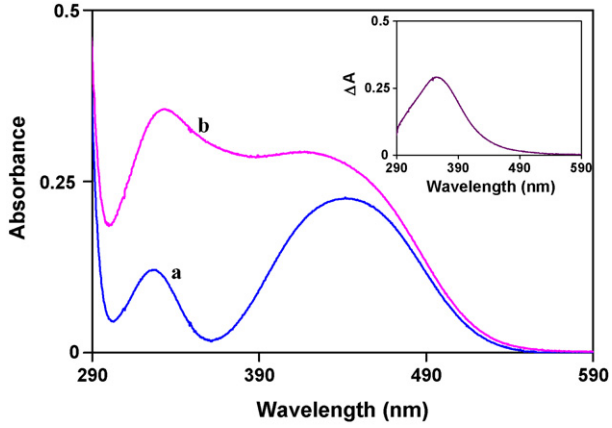

Fig. 3. Electronic absorption spectrum of Fc: (a) in pure tetrahydrofuran; (b) in a 2:3 (v:v) mixture of ethyl 2-cyanoacrylate and tetrahydrofuran. Inset shows the difference spectrum of (a) and (b). Reproduced from Ref. [9]. Copyright 2002 American Chemical Society.

Table 1
Electronic absorption spectral data for ferrocene compounds[a]

Compound[b]	Solvent	λ_{max} (nm), ε (M^{-1} cm^{-1})	
		Band 1	Band 2
Fc	Methanol	442 (91.5)	325 (51.3)
Fc	Isooctane	440 (95)	326 (55)
BFc	Methanol	483 (903)	363 (1360)
BFc	Acetonitrile	472 (780)	358 (1340)
BFc	Isooctane	459 (610)	355 (1220)
BFc-3Me	Methanol	483 (783)	355 (1360)
BFc–Cl	Methanol	483 (885)	358 (1340)
DFc	Methanol	486 (943)	353 (2090)
DFc	Acetonitrile	480 (885)	353 (2240)
DFc	Cyclohexane	469 (713)	352 (2020)
DFc	Isooctane	470 (700)	354 (1970)
DFc-*o*-Me	Methanol	483 (898)	346 (2080)
DFc-*m*-Me	Methanol	486 (945)	353 (2100)
DFc–3Me	Methanol	486 (852)	345 (2160)
DFc–Cl	Methanol	486 (915)	347 (2170)
DFc–Cl	Cyclohexane	473 (672)	346 (1900)
DFc–F	Methanol	484 (963)	349 (2180)

[a] Data from Ref. [26].
[b] See Fig. 1 for structures.

field transitions. Moreover, because such transitions involve an angular redistribution of electron density centered on the metal rather than a vectorial displacement of charge between the metal and ligands, the bands undergo only minor shifts in energy as a function of solvent polarity (Table 1).

Higher-energy features in the electronic absorption spectrum of Fc arise from intramolecular charge transfer transitions. In isopentane, the intense band at 200 nm has been assigned as ligand-to-metal charge transfer (LMCT) in character [17]. Shoulders observed at 265 nm and 240 nm have been attributed to LMCT and metal-to-ligand charge transfer (MLCT) transitions, respectively [18].

Despite possessing several potentially reactive ligand field and charge transfer excited states, Fc undergoes no discernible photoinduced metal-ring bond cleavage or redox processes in non-halogenated solvents such as cyclohexane, acetone, and methanol [19]. This lack of reactivity suggests that these excited states undergo very rapid electronic and vibrational relaxation to the ground state. The absence of luminescence from Fc supports this interpretation.

Ferrocene exhibits additional spectral and photochemical features when dissolved in a good electron-accepting solvent such as a halogenated hydrocarbon [20] or ethyl 2-cyanoacrylate (CA) [9]. The metallocene and solvent form a photoactive ground-state donor–acceptor complex, a process often accompanied by the appearance of an absorption band characteristic of the new species (Fig. 3, spectrum b and inset). Given the ease of oxidizing Fc and the electron-accepting character of the solvent, this band has been attributed to an intermolecular charge-transfer-to-solvent (CTTS) transition. Direct support for this assignment is provided by the observation that irradiating the complex in the wavelength region of this transition causes the one-electron oxidation of Fc to the ferricinium cation and reduction of the solvent

to its corresponding radical anion (Eq. (3)). Secondary reactions of these photogenerated species lead to permanent products [21–23]. When the solvent is CA, the radical anion formed in the primary photochemical process functions as an effective initiator for the anionic polymerization of the cyanoacrylate monomer (Eq. (4)) [9].

$$\mathrm{Fc} + \mathrm{CA} \rightleftarrows \underset{\text{donor–acceptor complex}}{[\mathrm{Fc}, \mathrm{CA}]} \xrightarrow{h\nu} \mathrm{Fc}^{+} + \mathrm{CA}^{\bullet -} \quad (3)$$

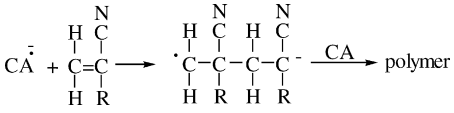

(4)

2.2. Ruthenocene

This $4d^6$ metallocene (Rc in Fig. 1) adopts a sandwich structure with an eclipsed orientation of the cyclopentadienyl rings. Applying the same type of analysis used earlier for Fc leads to the prediction of three spin-allowed ligand field transitions for Rc : $^1A_1' \rightarrow a^1E_1'$, $^1A_1' \rightarrow {}^1E_2'$, and $^1A_1' \rightarrow b^1E_1'$. The first two transitions overlap and contribute to the weak band observed at 321 nm in room-temperature methanol (Fig. 4). The third transition gives rise to the weak band at 278 nm. Higher-energy absorption features have been attributed to intramolecular MLCT or LMCT transitions [17]. Weak phosphorescence from a ligand field triplet state of Rc has been observed at low temperature [24,25].

The photochemical behavior of Rc is very similar to that of Fc. The 4d metallocene is photoinert in non-halogenated media, but it can form a photoactive ground-state donor–acceptor complex with a good electron-accepting solvent such as CA [9]. The complex exhibits an absorption band in the near ultraviolet region that arises from a CTTS transition. Irradiation at wavelengths that excite this transition results in oxidation of Rc and reduction of the solvent (analogous to the behavior described by Eq. (3)). The radical anion generated via this photoredox process then initiates the anionic polymerization of the monomer (Eq. (4)).

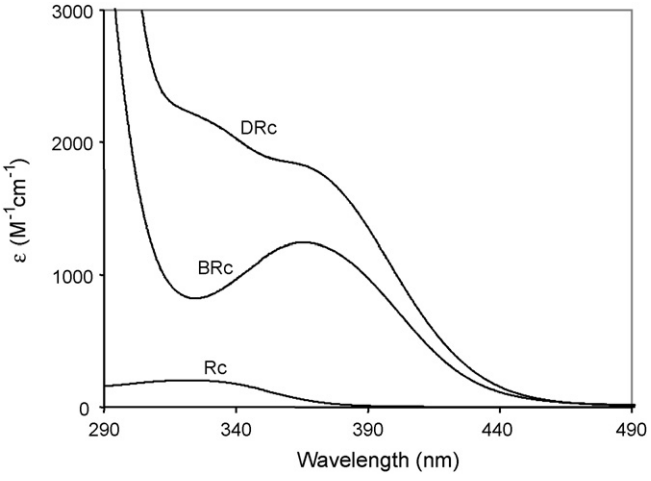

Fig. 4. Electronic absorption spectra of Rc, BRc, and DRc in room-temperature methanol. Reproduced from Ref. [36]. Copyright 2005 American Chemical Society.

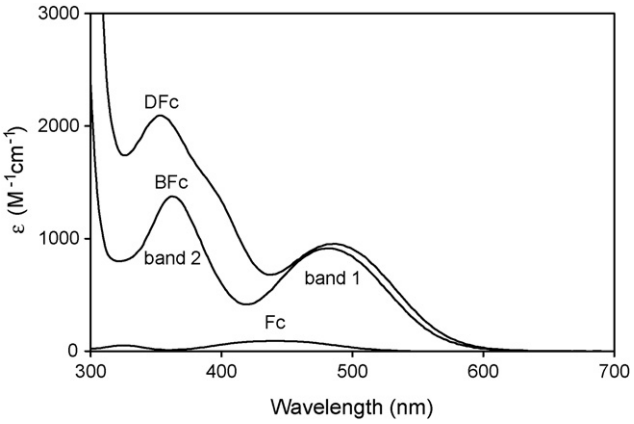

Fig. 5. Electronic absorption spectra of Fc, BFc, and DFc in room-temperature methanol. Reproduced from Ref. [27]. Copyright 2003 American Chemical Society.

3. Spectroscopy and photochemistry of benzoyl-substituted group 8 metallocenes

3.1. Benzoyl-substituted ferrocenes

Adding an electron-withdrawing benzoyl group to one or both cyclopentadienyl rings of ferrocene causes a significant perturbation of electronic properties [19,26,27]. This substituent effect is evident from the electronic absorption spectra of the representative complexes shown in Fig. 5 and the spectral data compiled in Table 1. In contrast to the weak ligand field bands displayed by Fc, the benzoyl-substituted derivatives exhibit bands (designated 1 and 2) at longer wavelengths and with significantly higher intensities. Moreover, the maximum of band 1 undergoes a significant bathochromic shift in more polar solvents (Table 1). We have attributed these spectral characteristics of benzoyl-substituted ferrocenes to the mixing of appreciable metal-to-ligand charge transfer character into their low-energy electronic excited states. This MLCT contribution can be represented by a limiting resonance structure of the type depicted in Fig. 6, where the formal charges on iron and oxygen signify the vectorial displacement of electron density from the metal to the ligand. Conjugation between the π orbitals of the cyclopentadienyl and phenyl rings and the adjacent carbonyl group allows the

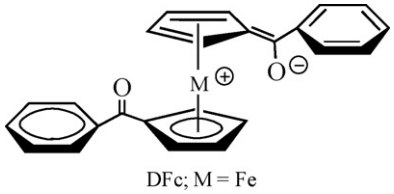

Fig. 6. Resonance structure depicting the MLCT character of the low-energy electronic excited states of benzoyl-substituted group 8 metallocenes. Formal charges on atoms are circled. Reproduced from Ref. [36]. Copyright 2005 American Chemical Society.

transferred charge to be delocalized over several atoms, thus stabilizing the MLCT excited state relative to the ground state and lowering the transition energy [28]. Polar solvents also lower the transition energy owing to the greater Coulombic stabilization of the dipolar (charge-separated) excited state. Mixing charge transfer character into the transition lessens its Laporte forbidden character and thereby increases the intensity of the absorption band.

Further evidence that the low-energy electronic absorption bands of benzoyl-substituted ferrocenes contain MLCT character is provided by resonance Raman spectroscopy. Charge transfer transitions are particularly effective for inducing intensity enhancement of the Raman-active vibrational modes of chromophores when the excitation frequency lies within the absorption envelope. Moreover, to a first approximation, this resonant enhancement is most pronounced for vibrations that mimic the distortion in the electronic excited state populated [29]. Referring to the excited-state resonance structure shown in Fig. 6, we expect that excitation into the low-energy absorption bands of benzoyl-substituted ferrocenes should cause selective enhancement of in-plane vibrations of the cyclopentadienyl and phenyl rings owing to changes in conjugation between the two rings, as well as strong enhancement of the carbonyl vibrational mode due to lengthening of the C–O bond.

These expectations are borne out by the low-temperature solid-state Raman spectra of BFc shown in Fig. 7 (similar results are obtained for DFc), where the band intensities measured at each excitation wavelength have been normalized relative to the non-resonantly enhanced band of the sulfate ion at 985 cm^{-1} [27]. The preresonance spectrum obtained with 647-nm excitation is dominated by the 1624 cm^{-1} band corresponding to the ν(C–O) stretching mode of the benzoylcyclopentadienyl ligand and the 1105 cm^{-1} band arising from the ν(C–C) symmetric breathing mode of the unsubstituted cyclopentadienyl ring. All other bands are readily assigned to internal modes of the benzoylcyclopentadienyl ligand. Excitation at 568 nm into the low-energy tail of electronic absorption band 1 selectively enhances the Raman intensities of the C–O stretching mode and other vibrations associated with the benzoylcyclopentadienyl ligand. In contrast, no resonant enhancement occurs for the 1105 cm^{-1} band of the unsubstituted cyclopentadienyl ring. These results are fully consistent with the bonding changes expected upon populating an excited state containing appreciable MLCT character.

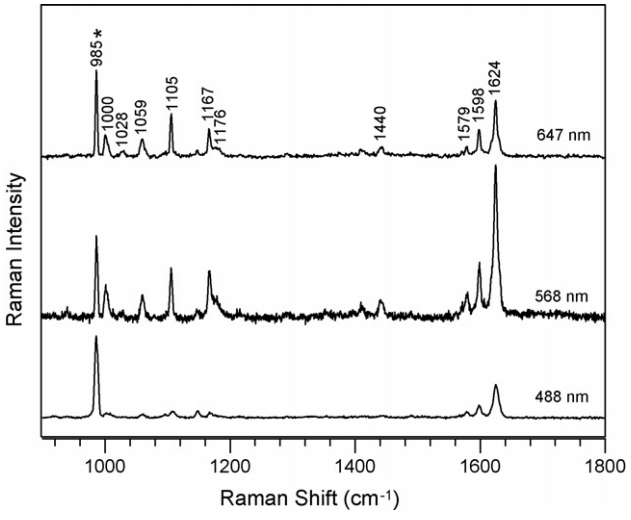

Fig. 7. Solid state, low-temperature (17 K) Raman spectra of BFc using 488-, 568-, and 647-nm excitation. The Raman intensities at each excitation wavelength have been normalized to the intensity of the sulfate band at 985 cm^{-1} (marked with an asterisk). Reproduced from Ref. [27]. Copyright 2003 American Chemical Society.

Excitation at 488 nm near the low-energy absorption band maximum of BFc causes extensive sample decomposition as evidenced by the substantially lower intensities of all Raman bands relative to the sulfate standard (Fig. 7). We have proposed that this photoreactivity is another consequence of mixing MLCT character into the low-energy excited states of the benzoyl-substituted ferrocenes [26,27]. Examination of the resonance structure in Fig. 6 reveals that this charge transfer contribution formally reduces the hapticity of a cyclopentadienyl ring from η^5 to η^4, thereby weakening ring-metal bonding. Furthermore, the enhanced eletrophilicity of the metal center assists the formation of bonds to incoming ligands. Both of these photoinduced changes in electron density should facilitate the loss of a benzoylcyclopentadienide anion.

We have investigated the solution photochemistry of benzoyl-substituted ferrocenes in considerable detail [26,27]. In one study, an acetonitrile (AN) solution containing DFc and Na^+ (as the carrier cation) was irradiated in the transparent tip of an electrospray ionization mass spectrometer system. As seen in Fig. 8, the mass spectrum of the photolyte contains three major product series: (1) adducts of benzoylcyclopentadiene and a proton (m/z = 171.1) or a sodium ion (m/z = 193.0 and 363.1); (2) adducts of half-sandwich iron(II) complexes and a proton (m/z = 154.0 and 174.5); (3) fully ring-deligated iron(II) complexes of general formula $[Fe(AN)_n]^{2+}$ (m/z = 89.5, 110.0, and 130.5 for n = 3, 4, and 5, respectively). Observation of the first two product series strongly supports the assignment of heterolytic metal-ring bond cleavage (Eq. (5); L denotes a solvent molecule) as the primary photochemical reaction of DFc.

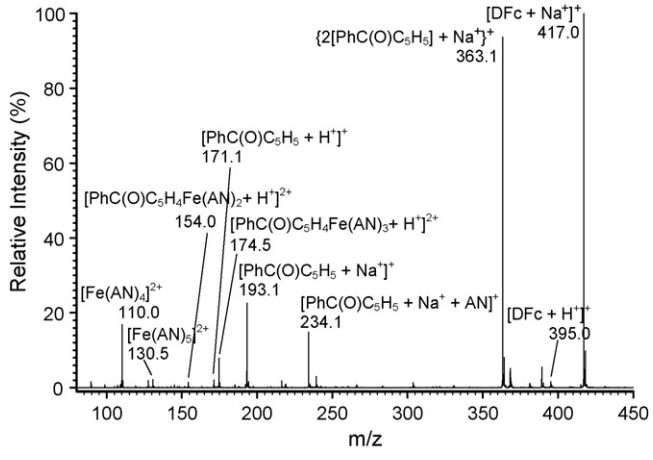

Fig. 8. Electrospray ionization mass spectrum of a photolyzed (488 nm) acetonitrile solution originally containing 130 μM DFc and 120 μM Na^+. Reproduced from Ref. [27]. Copyright 2003 American Chemical Society.

Table 2
Disappearance quantum yield (ϕ_{dis}) data

Run[a]	Compound[b]	ϕ_{dis}[c]
1	BFc	0.083
2	BFc–Cl	0.098
3	DFc	0.42 ± 0.06
4	DFc[d]	0.37 ± 0.02
5	DFc[e]	0.36 ± 0.01
6	DFc[f]	$<10^{-4}$
7	DFc-*o*-Me	0.41 ± 0.02
8	DFc-*m*-Me	0.41 ± 0.02
9	DFc–3Me	0.34 ± 0.00
10	DFc–Cl	0.41 ± 0.01
11	DFc–F	0.47 ± 0.02

[a] Experimental conditions: excitation wavelength, 546 nm unless noted otherwise; temperature, $22 \pm 2^{\circ}$ C; solvent, methanol unless noted otherwise; deoxygenation by bubbling with argon did not change ϕ_{dis}.
[b] See Fig. 1 for structures.
[c] Where quoted, error limit represents mean deviation of two or more runs. Estimated accuracy of ϕ_{dis} is 10–15%.
[d] Excitation wavelength is 488 nm.
[e] Excitation wavelength is 406 nm.
[f] Excitation wavelength is 488 nm; solvent is cyclohexane.

The benzoylcyclopentadienide anion released in this process is sufficiently basic to abstract a proton from ambient traces of water or other protic impurities, thereby producing the neutral 1-benzoyl-1,3-cyclopentadiene molecule. The carbonyl oxygen atom of the benzoyl group forms Lewis acid–base adducts with a proton or a sodium ion to yield the ionic products detected. Half-sandwich complexes also contain a basic carbonyl oxygen and undergo adduct formation with a proton to yield the dicationic species observed. The fully ring-deligated iron(II) complexes that comprise the third photoproduct series most likely result from thermal decomposition of the initially-formed half-sandwich complex.

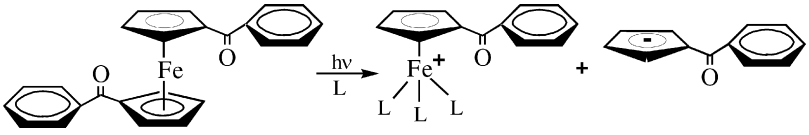

(5)

Disappearance quantum yield (ϕ_{dis}) data compiled in Table 2 reveal that the number of benzoyl-substituted rings present in a ferrocene molecule is a key determinant of its excited-state reactivity. Thus, 1,1′-dibenzoylferrocenes generally undergo loss of a benzoylcyclopentadienide anion much more efficiently than their monobenzoylferrocene analogues. Substituents on the phenyl ring of the benzoyl group exert relatively little influence on this ring-loss process. The electron-withdrawing fluorine atoms in DFc–F increase ϕ_{dis} relative to the electron-releasing methyl groups in DFc-*o*-Me (runs 11 and 7), but the effect is modest. Steric effects also may contribute to the smaller ϕ_{dis} value for DFc–3Me (run 9), since this is the only complex studied that contains two ortho substituents on each phenyl ring for shielding the metal from attack by entering solvent molecules.

Values of ϕ_{dis} remain reasonably constant over a range of excitation wavelengths that encompass absorption bands 1 and 2 of DFc (Table 2, runs 3–5). This behavior suggests that the initially populated Franck–Condon excited state undergoes very rapid electronic and vibrational relaxation to yield a common thermally equilibrated excited (thexi) state of the metallocene. Metal-ring bond cleavage then occurs from this thexi state directly or from a close lying reactive state reached by thermal upconversion [30]. Solvent plays an important role in the photochemical process as evidenced by the sharp decrease in ϕ_{dis} upon switching from methanol to cyclohexane (compare runs 4 and 6). We have suggested that photoinduced loss of the benzoylcyclopentadienide ligand proceeds via a succession of ring-slipped intermediates such as the η^5,η^3 complex shown in Eq. (6) [26,27]. Solvent can assist in the formation of this species by attacking the electrophilic metal center in the excited state and partially displacing the five-membered ring. The η^5,η^3 intermediate then has the option of reacting further with solvent to yield the half-sandwich product or expelling the coordinated solvent to regenerate the parent complex. Strongly coordinating solvents such as methanol favor the former path, which leads to a high value for ϕ_{dis}, whereas poorly coordinating solvents such as cyclohexane favor the latter path and a low ϕ_{dis} value. When a benzoyl-substituted ferrocene is irradiated in neat CA, the liberated benzoylcyclopentadienide serves as a potent initiator for the anionic polymerization of the monomer [7].

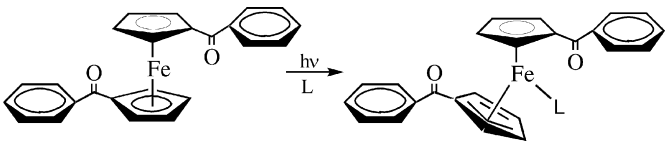

(6)

Some intriguing similarities exist between the electronic properties of benzoyl-substituted ferrocenes and their highly-strained analogues, the [1] ferrocenophanes, as exemplified by the phosphorus-bridged complex, **1** (Eq. (7)). Typically, the lowest energy band in the electronic absorption spectrum of a [1] ferrocenophane is red-shifted and more intense than the lowest ligand field band in Fc [31]. Molecular orbital calculations [32] attribute this behavior to the bridge-induced tilting of the cyclopentadienyl rings, which decreases the energy gap between the highest occupied and lowest unoccupied molecular orbitals of the [1] ferrocenophane. Most importantly, this tilting imparts a degree of MLCT character to the electronic transition between these orbitals. Irradiation of a [1] ferrocenophane complex in a nucleophilic medium results in cyclopentadienyl ring slippage and, ultimately, metal-ring bond cleavage to generate intermediates that react further with the parent complex to yield a ring-opened metallopolymer (Eq. (7)) [33–35]. This behavior lends further credence to our earlier generalization that mixing MLCT character into the low-energy electronic excited states of

Table 3
Solvent dependence of the electronic absorption spectrum of BRc[a]

Solvent	Dielectric constant	λ_{max}[b] (nm)	ε_{max} ($M^{-1}\,cm^{-1}$)
Methanol	32.7	365	1250
Acetonitrile	37.5	356	977
Cyclohexane	2.02	342	1020
Carbon tetrachloride	2.24	345	1320
Chloroform	4.81	358	1340

[a] Reproduced from Ref. [36]. Copyright 2005 American Chemical Society.
[b] Maximum of low-energy absorption band.

ferrocene derivatives facilitates photoinduced ring loss.

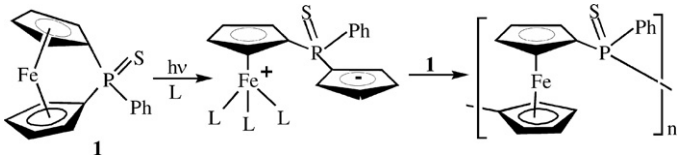

(7)

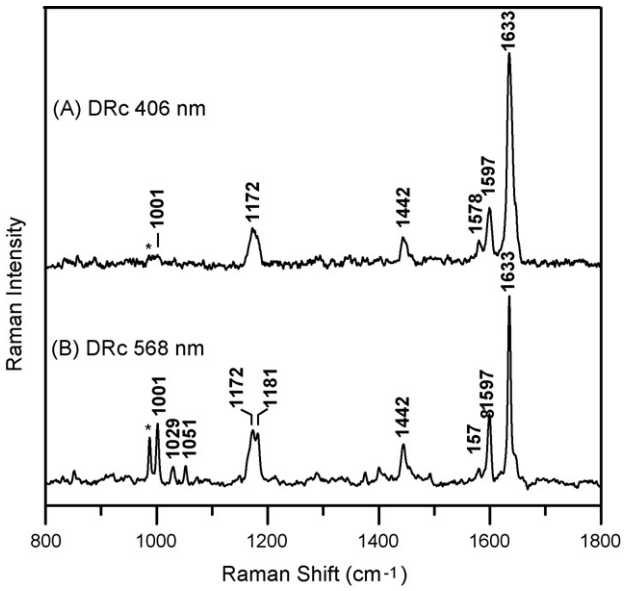

Fig. 9. Solid state, low-temperature (17 K) Raman spectra of DRc. The asterisk marks the sulfate band at 985 cm^{-1}, which is used as an internal standard for the extent of resonance enhancement. Reproduced from Ref. [36]. Copyright 2005 American Chemical Society.

3.2. Benzoyl-substituted ruthenocenes

Changes in electronic absorption spectra resulting from the addition of a benzoyl group to one or both rings of Rc are shown in Fig. 4 [36]. Both BRc and DRc (see Fig. 1 for structures) exhibit bands at longer wavelengths and with significantly higher intensities than the parent metallocene. Moreover, band positions depend upon the polarity of the solvent (Table 3). Using arguments identical to those presented earlier for the corresponding ferrocene compounds, we attribute these spectral characteristics to the mixing of metal-to-ligand charge transfer character into the low-energy electronic excited states of benzoyl-substituted ruthenocenes. Supporting evidence for the importance of this MLCT contribution again is provided by resonance Raman spectroscopy [36]. The relative intensities of the Raman bands observed for DRc (Fig. 9; similar behavior occurs for BRc) change dramatically with respect to each other and the sulfate internal standard when comparing spectra obtained using non-resonant (568 nm) and resonant (406 nm) excitation. Intensity enhancement occurs selectively for vibrations of the benzoylcyclopentadienyl ligand, with the largest enhancement being observed for the C–O stretching mode at 1633 cm^{-1}. These results are consistent with the bonding changes expected to occur following the population of an excited state containing significant MLCT character (Fig. 6).

While absorption band positions are sensitive to changes in solvent, no feature attributable to a CTTS transition is evident above 300 nm in the spectra of BRc or DRc measured in CA or halogenated media. Instead, the spectra vary in a manner that correlates reasonably well with solvent polarity. Thus the low-energy band occurs at very similar wavelengths in the nonpolar media cyclohexane and carbon tetrachloride, but shifts to longer wavelength in the more polar chloroform (Table 3). We conclude from these results that CTTS transitions of benzoyl-substituted ruthenocenes in good electron-accepting solvents occur at relatively high energy and are effectively masked by the more intense bands containing MLCT character.

Prolonged irradiation of BRc or DRc in methanol, acetonitrile, or cyclohexane causes no discernible change in the electronic absorption spectrum. These results allow us to place an upper limit of 4×10^{-4} on the quantum yield for photoinduced ring loss. This striking lack of photoreactivity was confirmed in another set of experiments that employed electrospray ionization mass spectrometry to analyze samples. No peaks attributable to half-sandwich compounds or other photoproducts were observed in the mass spectra of photolyzed acetonitrile solutions of the metallocenes. Collectively, these results indicate that BRc and DRc are photoinert in poor electron-accepting media. This photoinertness correlates with the greater ground-state metal-ring bond strength of 4d versus 3d metallocenes [3], suggesting that the photoexcited ruthenocene compounds retain sufficient bonding to prevent ring loss. Moreover, the residual bonding in the excited state may be enhanced by η^6-fulvene coordination of the labilized ring as depicted in Fig. 10 [37]. This coordination mode should be more important in BRc and DRc than in the corresponding ferrocenes owing to the greater radial extension of 4d versus 3d orbitals and the resulting better overlap with the exocyclic double bond of the fulvene moiety.

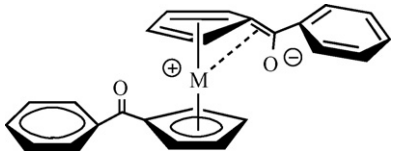

Fig. 10. Resonance structure depicting η^6-fulvene bonding of the labilized ring in the low-energy electronic excited states of benzoyl-substituted group 8 metallocenes. Formal charges on atoms are circled. Reproduced from Ref. [36]. Copyright 2005 American Chemical Society.

While BRc and DRc resist photoinduced metal-ring bond cleavage, both compounds function as photoinitiators for the anionic polymerization of CA. We turn next to a discussion of the mechanism of photoinitiation by these and the other group 8 metallocenes discussed in this article.

4. Anionic polymerization using group 8 metallocene photoinitiators

Our original impetus for studying the spectroscopy and photochemistry of Fc, Rc, and their benzoyl-substituted derivatives arose from the search for new anionic photoinitiators [8,10]. These group 8 metallocenes possess several attractive properties including solubility in a broad range of nonaqueous solvents, excellent thermal stability, and absorption in the ultraviolet and visible wavelength regions. Moreover, earlier studies indicated these compounds undergo photochemical reactions that release anionic species [38]. For these reasons, we investigated their behavior as photoinitiators for the polymerization of ethyl 2-cyanoacrylate.

Solutions of neat CA containing millimolar concentrations of Fc, Rc, or one of their benzoyl-substituted derivatives undergo no discernible change in viscosity for at least 24 h when stored in the dark at room temperature. Upon being irradiated with polychromatic light, however, these solutions polymerize to a hard, plastic-like solid. Representative plots of percent polymerization versus irradiation time are displayed in Fig. 11 for samples of CA containing Rc. Plots with very similar characteristics are obtained for the other metallocene photoinitiators tested [36]. Typically, polymerization exhibits an induction period that depends upon light intensity (compare curves b and c) and the quantum efficiency of generating the active initiating species. Thereafter, polymerization accelerates rapidly before finally approaching a plateau at 75–85% conversion. The induction period arises from the presence in the commercial monomer of an acid stabilizer, which scavenges adventitious traces of basic

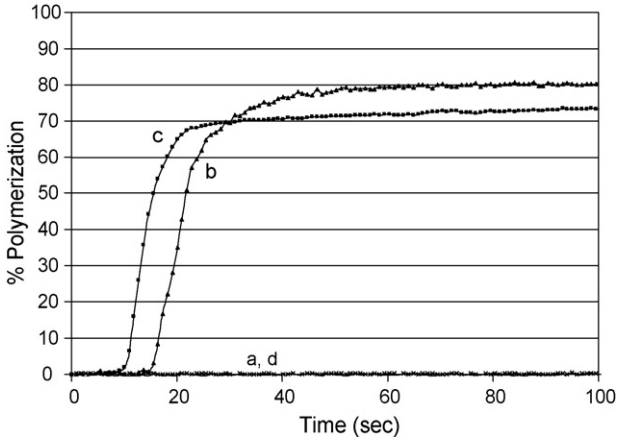

Fig. 11. Plots of percent polymerization vs. time for samples of CA containing 10.0 mM Rc: (a) non-irradiated, (b) irradiated with 33 mW/cm^2 of polychromatic light, (c) irradiated with 117 mW/cm^2 of polychromatic light, (d) irradiated with 117 mW/cm^2 of polychromatic light after addition of 133 ppm of methanesulfonic acid. Reproduced from Ref. [36]. Copyright 2005 American Chemical Society.

Table 4
Maximum rate (R_p) data for photoinitiated polymerization of CA[a]

Photoinitiator[b]	Concentration (mM)	Light intensity (mW/cm^2)	R_p (M/s)
Fc	9.6	110	0.060
DFc	2.7	30	1.7
Rc	10.0	33	0.56
Rc	10.0	117	0.94
BRc	10.5	126	0.68
DRc	11.6	105	0.14

[a] Reproduced from Ref. [36]. Copyright 2005 American Chemical Society.
[b] See Fig. 1 for structures.

impurities. Polymerization is inhibited until enough anionic species are photochemically generated to neutralize this acid, whereupon rapid consumption of monomer commences. In support of this interpretation, we find that adding extra acid to a sample lengthens the induction period (compare curves c and d) and slows the ensuing anionic polymerization.

The rate of photoinitiated polymerization, R_p, at any point during a run can be determined from the conversion-time plots. To establish a common basis for making comparisons, we calculated the maximum rate attained with each photoinitiator during the acceleratory period of the polymerization process. These data, which are compiled in Table 4, reveal two contrasting trends. First, for the ferrocene compounds, R_p decreases in the order DFc > Fc, indicating that the presence of a benzoyl group has a salutary effect on the rate of photoinitiated polymerization. This result agrees with prior observations that CA solutions containing DFc or BFc require shorter irradiation times to undergo a visually detectable change in viscosity than solutions containing Fc [5]. Second, the benzoyl group has the exact opposite effect within the ruthenocene series, with R_p decreasing in the order Rc > BRc > DRc.

This reversal in the trends of R_p values for corresponding $3d^6$ and $4d^6$ metallocene photoinitiators can be understood in terms of the competition between the two charge-transfer-induced pathways that yield the active initiating species: intermolecular metallocene → CA electron transfer, which produces the radical anion of CA (Eq. (3)) versus intramolecular heterolytic metal-ring bond cleavage, which affords the benzoylcyclopentadienide anion (Eq. (5)). Electron-rich Fc favors the former pathway, while BFc and DFc, which bear the electron-withdrawing benzoyl group, prefer the latter. The observed trend in the maximum rate of photoinitiated polymerization, DFc > BFc > Fc, reflects the contributions of two factors. First, the MLCT bands of BFc and DFc possess higher molar absorptivities and extend over a broader wavelength range than the CTTS band of the [Fc, CA] donor–acceptor complex (compare spectra in Figs. 3 and 5). Consequently, the benzoyl-substituted derivatives can use a larger fraction of the incident radiation in forming the active initiating species. Second, the photochemical reaction that generates the initiating species occurs with higher quantum efficiency for DFc than for BFc (Table 2) [26].

Both photoinitiation pathways are available to the ruthenium-containing metallocenes, but strong metal-ring bonding precludes efficient heterolytic bond cleavage. Hence, only photoin-

duced metallocene → CA electron transfer should be effective in producing the initiating species. While a CTTS band is not evident in the absorption spectrum of BRc or DRc dissolved in CA, the maximum rate of photoinitiated polymerization and the ease of oxidizing the metal center [39] follow the same trend, Rc > BRc > DRc. This correlation between photoinitiation and redox properties supports a mechanism whereby photoinduced metallocene → CA electron transfer generates the active initiating species, which, by analogy to Eq. (3), is assigned as the CA radical anion.

5. Summary and outlook

Considerable progress has been made in understanding the electronic structures and excited state reactivities of group 8 metallocenes. Several key findings are summarized below.

(i) Fc and Rc are photoinert in poor electron-accepting solvents such as cyclohexane and methanol. This behavior is somewhat surprising given the potentially reactive ligand field and intramolecular charge transfer excited states populated under these conditions.
(ii) Fc and Rc form a photoactive ground-state donor–acceptor complex in good electron-accepting media such as halogenated hydrocarbons and ethyl 2-cyanoacrylate. Populating the CTTS excited state of the complex results in oxidation of the metallocene and reduction of the solvent.
(iii) Placing a benzoyl group on one or both rings of Fc and Rc introduces MLCT character into the low-energy excited states of the resulting derivatives.
(iv) This MLCT contribution facilitates heterolytic metal-ring bond cleavage in benzoyl-substituted ferrocenes. In contrast, strong residual bonding in the excited states of the corresponding ruthenocenes renders them photoinert to ring loss.
(v) Group 8 metallocenes undergo two photochemical reactions that generate an active initiating species for the anionic polymerization of CA: intermolecular metallocene → CA electron transfer (Eq. (3)) from a CTTS excited state, and intramolecular heterolytic metal-ring bond cleavage (Eq. (5)) from a state containing MLCT character. Fc, Rc, BRc, and DRc favor the first process, while benzoyl-substituted ferrocenes prefer the second.
(vi) The generalization that mixing MLCT character into the low-energy electronic excited states of ferrocene derivatives facilitates photoinduced metal-ring bond cleavage appears to apply to highly-strained [1] ferrocenophanes.

Future studies from this laboratory will explore the spectroscopy and photochemistry of the 5d metallocenes—osmocene, benzoylosmocene, and 1,1′-dibenzoylosmocene. Several related questions will be addressed. Does the presence of the benzoyl group introduce MLCT character into the low-energy electronic excited states of the latter two compounds? Do these compounds undergo photoinduced ring loss analogous to Eq. (5), or does strong residual metal-ring bonding in the excited state render them photoinert? Are osmocene and its benzoyl-substituted derivatives effective as anionic photoinitiators, and, if they are, by what mechanism(s)? Comparing the results of these studies with those obtained for the corresponding ferrocene and ruthenocene compounds should lead to a better understanding of the electronic factors that influence the spectral and photochemical behavior of group 8 metallocenes.

Acknowledgments

We are grateful to Professors I. Jonathan Amster, Richard A. Dluhy, and Michael K. Johnson, and members of their groups for useful discussions and technical assistance. JSR Corporation and the University of Georgia Research Foundation provided financial support for our work. Acknowledgment also is made to the donors of the Petroleum Research Fund, administered by the American Chemical Society, for financial assistance.

References

[1] T.J. Kealy, P.L. Pauson, Nature (London) 168 (1951) 1039.
[2] S.A. Miller, J.A. Tebboth, J.F. Tremaine, J. Chem. Soc. (1952) 633.
[3] N.J. Long, Metallocenes: An Introduction to Sandwich Complexes, Blackwell Science, London, 1998.
[4] A. Togni, T. Hayashi (Eds.), Ferrocenes, VCH, Weinheim, 1995.
[5] Y. Yamaguchi, B.J. Palmer, C. Kutal, T. Wakamatsu, D.B. Yang, Macromolecules 31 (1998) 5155.
[6] Y. Yamaguchi, C. Kutal, in: G. Ondrejovič, A. Sirota (Eds.), Coordination Chemistry at the Turn of the Century Slovak Technical University Press Bratislava 1999, p. 209.
[7] Y. Yamaguchi, C. Kutal, Macromolecules 33 (2000) 1152.
[8] C. Kutal, Coord. Chem. Rev. 211 (2001) 353.
[9] C.T. Sanderson, B.J. Palmer, A. Morgan, M. Murphy, R.A. Dluhy, T. Mize, I.J. Amster, C. Kutal, Macromolecules 35 (2002) 9648.
[10] C. Kutal, Y. Yamaguchi, W. Ding, C.T. Sanderson, X. Li, G. Gamble, I.J. Amster, in: K.D. Belfield, J.V. Crivello (Eds.), Photoinitiated Polymerization, ACS Symposium Series, No. 847, American Chemical Society, Washington, DC 2003 (Chapter 29).
[11] C. Kutal, in: M. Chanon (Ed.), Homogeneous Photocatalysis, John Wiley Chichester, UK, 1997 (Chapter 5).
[12] E. Reichmanis, F.M. Houlihan, O. Nalamasu, T.X. Neenan, Chem. Mater. 3 (1991) 394.
[13] D.B. Yang, C. Kutal, in: S.P. Pappas (Ed.), Radiation Curing: Science and Technology, Plenum Press, New York, 1992 (Chapter 2).
[14] F.A. Cotton, G. Wilkinson, Advanced Inorganic Chemistry, 5th ed., John Wiley, New York, 1988, p. 79.
[15] K.D. Warren, Struct. Bond. (Berlin) 27 (1976) 45.
[16] D.W. Clack, K.D. Warren, Struct. Bond. (Berlin) 39 (1980) 1.
[17] Y.S. Sohn, D.N. Hendrickson, H.B. Gray, J. Am. Chem. Soc. 93 (1971) 3603.
[18] N. Rösch, K.H. Johnson, Chem. Phys. Lett. 24 (1974) 179.
[19] A.M. Tarr, D.M. Wiles, Can. J. Chem. 46 (1968) 2725.
[20] J.C.D. Brand, W. Snedden, Trans. Faraday Soc. 53 (1957) 894.
[21] O. Traverso, F. Scandola, Inorg. Chim. Acta 4 (1970) 493.
[22] T. Akiyama, Y. Hoshi, S. Goto, A. Sugimori, Bull. Chem. Soc. Jpn. 46 (1973) 1851.
[23] T. Akiyama, A. Sugimori, H. Hermann, Bull. Chem. Soc. Jpn. 46 (1973) 1855.
[24] G.A. Crosby, G.D. Hager, K.W. Hipps, M.L. Stone, Chem. Phys. Lett. 28 (1974) 497.
[25] M.S. Wrighton, L. Pdungsap, D.L. Morse, J. Phys. Chem. 79 (1975) 66.
[26] Y. Yamaguchi, C. Kutal, Inorg. Chem. 38 (1999) 4861.
[27] W. Ding, C.T. Sanderson, R.C. Conover, M.K. Johnson, I.J. Amster, C. Kutal, Inorg. Chem. 42 (2003) 1532.
[28] J.A. Treadway, B. Loeb, R. Lopez, P.A. Anderson, F.R. Keene, T.J. Meyer, Inorg. Chem. 35 (1996) 2242.

[29] T.G. Spiro, R.S. Czernuszewicz, in: L. Que Jr. (Ed.), Physical Methods in Bioinorganic Chemistry: Spectroscopy and Magnetism, University Science Books, Sausalito, CA, 2000, p. 59.
[30] A. Vlček Jr., Coord. Chem. Rev. 177 (1998) 219.
[31] R. Rulkens, D.P. Gates, D. Balaishis, J.K. Pudelski, D.F. McIntosh, A.J. Lough, I. Manners, J. Am. Chem. Soc. 119 (1997) 10976.
[32] S. Barlow, M.J. Drewitt, T. Dijkstra, J.C. Green, D. O'Hare, C. Whittingham, H.H. Wynn, D.P. Gates, I. Manners, J.M. Nelson, J.K. Pudelski, Organometallics 17 (1998) 2113.
[33] T. Mizuta, M. Onishi, K. Miyoshi, Organometallics 19 (2000) 5005.
[34] T. Mizuta, Y. Imamura, K. Miyoshi, J. Am. Chem. Soc. 125 (2003) 2068.
[35] M. Tanabe, I. Manners, J. Am. Chem. Soc. 126 (2004) 11434.
[36] C.T. Sanderson, J.A. Quinlan, R.C. Conover, M.K. Johnson, M. Murphy, R.A. Dluhy, C. Kutal, Inorg. Chem. 44 (2005) 3283.
[37] S. Barlow, A. Cowley, J.C. Green, T.J. Brunker, T. Hascall, Organometallics 20 (2001) 5351.
[38] G.L. Geoffroy, M.S. Wrighton, Organometallic Photochemistry, Academic Press, New York, 1979 (Chapter 5).
[39] J.A. Page, G. Wilkinson, J. Am. Chem. Soc. 74 (1952) 6149.